JOURNAL OF MATERIALS SCIENCE 33 (1998) 4797–4812

Matrix molecular orientation in fiber-reinforced polypropylene composites

D. M. DEAN, L. REBENFELD, R. A. REGISTER*
TRI/Princeton and Department of Chemical Engineering, Princeton University, Princeton, NJ 08544, USA

B. S. HSIAO†
DuPont Central R&D, Wilmington, DE 19880, USA

A distinctive crystalline morphology which develops in certain fiber-reinforced thermoplastics, termed "transcrystallinity", occurs as the result of dense nucleation of polymer crystals at the surface of reinforcing fibers. As these fiber-sponsored nuclei grow, they impinge upon one another, such that crystal growth occurs essentially perpendicular to the fiber axis. Previous studies concerning transcrystallized composites have generally focused on single-fiber composites or model systems. Our interest is in elucidating the crystal orientation in conventional fiber-reinforced composites, and in quantifying the fraction of transcrystallized matrix, where present. In the present work, we develop a wide-angle X-ray scattering (WAXS) technique to investigate composites formed from an isotactic polypropylene (PP) matrix with practical loading levels of unidirectional pitch-based carbon, polyacrylonitrile (PAN)-based carbon, or aramid fibers. The transcrystalline fraction of the crystalline matrix approaches 0.95 in pitch-based carbon composites and 0.50 in the aramid composites near fiber loadings of 30 vol %. In addition, a previously-unreported mode of matrix orientation is observed in composites containing the non-transcrystallizing PAN-based carbon fibers, arising from restrictions on the isotropic growth of PP crystallites by the unidirectional fibers. This "constrained growth" orientation can coexist with the transcrystallized matrix at lower fiber loadings. © *1998 Kluwer Academic Publishers*

1. Introduction

During the past several years there has been considerable interest in the structure and properties of fiber-reinforced thermoplastic composites. Much of this interest has arisen due to the ease with which thermoplastic composites can be processed relative to their more traditional thermosetting counterparts as well as to the high impact toughness and the extended shelf life that thermoplastic materials provide. However, in many thermoplastic systems, the issues of structure and processing are complicated by crystallization of the matrix material. In addition, some fiber/matrix combinations yield an unusual crystalline morphology near the surface of the reinforcing fibers [1–9]. This "transcrystalline" structure occurs as the result of dense nucleation of the thermoplastic matrix along the surface of the reinforcing fibers. It seems intuitive that this type of directional crystal growth, away from the fiber axis, would yield substantial molecular orientation within the transcrystalline layer (TCL), thus influencing the composite's mechanical properties. However, conflicting conclusions have been reached regarding the actual effect of transcrystallinity [1]. Some of this confusion stems from an inability to characterize the TCL within realistic composites. In the past, characterization of transcrystalline systems has relied heavily on optical microscopy, which is effective only for model systems such as isolated fibers in thin thermoplastic films, or sheets of thermoplastic material sandwiched between two surfaces [2, 3]. A few studies of transcrystalline systems have employed X-ray scattering but have dealt solely with model systems [4, 5].

Although transcrystallinity occurs in a number of polymer matrices ranging from poly(ethylene terephthalate) to poly(phenylene sulfide) [6–9], we have focused our investigation on transcrystallinity in fiber-reinforced isotactic polypropylene (PP). A semicrystalline thermoplastic, PP can form into three known crystalline polymorphs, the most common of which is the monoclinic α–PP form [10–14]. Less common is the hexagonal β–PP form [15, 16], and the least common is the orthorhombic γ–PP [17, 18]. In addition,

* To whom correspondence should be addressed.
† Current address: Department of Chemistry, State University of New York at Stony Brook, Stony Brook, NY 11974.

PP can develop into a smectic or "mesophase" polymorph after being quenched from the melt [19, 20]. In the present study, the composites show predominantly or exclusively the α-polymorph.

We describe here the use of wide angle X-ray scattering (WAXS) to probe the orientation which arises in fiber-reinforced isotactic PP composites, and use this technique to accurately quantify the amount of transcrystalline material within realistic unidirectional composites crystallized in the absence of matrix flow. By focusing on systems containing a practical level of fiber reinforcement, we hope to directly link the level of transcrystallinity to mechanical properties.

2. Experimental

2.1. Optical microscopy

A Zeiss transmission optical microscope employing crossed polarizers was used to observe the crystallization behavior in thin film specimens of the various fiber/polymer systems. Thin film samples were prepared by compression molding at 250 °C, under minimal pressure, individual filaments between thin films of the PP homopolymers, which in turn were placed between a glass coverslip and slide. The resulting samples were then placed in a Mettler FP80 hot stage where the specimens were re-melted at 250 °C for one min and then cooled at 11.5 °C/min to 110 °C. After crystallization of the PP matrix was complete, photos of the thin film samples were taken using 35 mm color film.

2.2. Composite sample preparation

Unidirectional, continuous-fiber-reinforced composites were prepared by compression-molding multiple filaments of either Kevlar®-29, pitch-based carbon, or polyacrylonitrile (PAN)-based carbon between thin films of PP in an aluminum mold. The fibers had nominal diameters of 12, 9, and 8 μm respectively. Untreated Kevlar®-29 and experimental pitch-based carbon fibers were provided by DuPont with respective tensile moduli of 71 and 688 GPa. Kevlar®-29 has a reported density of 1.45 g/cm^3 while the density of the experimental pitch-based carbon fibers was taken as the literature value of 2.1 g/cm^3 [21]. The untreated PAN-based carbon fibers (Hexcel AS-4) have a density of 1.8 g/cm^3 and a modulus of 227 GPa. Two different grades of additive-free isotactic PP homopolymer were provided by Montell Polyolefins along with their molecular weights: the 24 MFI has $M_w = 293$ kg/mol, the 400 MFI has $M_w = 104$ kg/mol, and both have polydispersity indices of 4.1. Both polymers were obtained in pellet form and were first compression-molded between aluminum plates at 250 °C into thin films before being quenched in a cold water bath. The density for the PP matrix within the composites was taken as that reported for the as-received pellets (0.907 g/cm^3).

For each composite sample, measuring $60 \times 30 \times 1$ mm, nineteen (19) layers of filaments were "sandwiched" between twenty (20) PP films, each film having an approximate thickness of 50 μm. This layered structure was then compression-molded at 250 °C for 25 min within a closed aluminum mold treated with a commercial release agent. The aluminum mold containing the composites, which varied in their fiber volume fraction, was then removed from the hot press and allowed to cool under ambient conditions. By measuring the mold temperature with a digital thermometer, the cooling rate was determined to average 11.5 °C/min over the range of 250 to 60 °C. An unreinforced sample of the 24 MFI PP, cooled at this rate from 250 °C in a Perkin-Elmer DSC-4, showed that under these conditions the onset of crystallization occurs at 110 °C. Each composite was then cut into 4 test specimens, measuring $30 \times 15 \times 1$ mm.

2.3. X-ray measurements

Two-dimensional WAXS patterns were obtained from unreinforced PP plaques as well as from the composite samples in a transmission geometry using an evacuated Statton camera manufactured by W. H. Warhus. X-rays with a source wavelength of 0.154 nm were produced using a sealed tube generator with Cu target and a Huber graphite monochromator. The WAXS patterns were recorded using Kodak® image plates (IP) with the IP storage phosphors being read by a Molecular Dynamics SI Phosphorimager.

From the scattering patterns, azimuthal traces of several PP unit-cell reflections were generated to quantify the orientation of the various crystal planes. Before the azimuthal traces were analyzed, the amorphous scattering intensity was subtracted from the crystalline reflection of interest by taking, at each azimuthal position, the average of the intensity at immediately lower and higher scattering angles about the crystalline reflection.

3. Results and discussion

3.1. Optical microscopy

Fig. 1 shows optical micrographs of isolated fibers in thin films of the 24 MFI PP. The pitch-based carbon fiber induces a dense population of PP crystal nuclei along its surface, as shown in Fig. 1a. This leads to oriented growth of the PP lamellae away from the fiber outward into the thermoplastic matrix, thus forming a transcrystalline layer (TCL). Fig. 1b shows that Kevlar fibers also sponsor a number of PP nuclei at their surface. By contrast, Fig. 1c shows that PAN-based carbon fibers do not nucleate the PP matrix. Changing the matrix to the 400 MFI PP yielded optical micrographs similar to those shown in Fig. 1. Hence, we infer that in our highly-loaded composites a TCL should develop in the pitch-based carbon and Kevlar systems but not in composites containing PAN-based carbon.

3.2. Transcrystalline orientation

3.2.1. Pitch-based carbon fibers

Fig. 2 presents the 2-D WAXS pattern from an unreinforced sample of the 24 MFI PP, which was molded in the same manner as the composite samples. As can be seen, the azimuthal intensity distribution for each reflection is uniform, confirming that the PP is

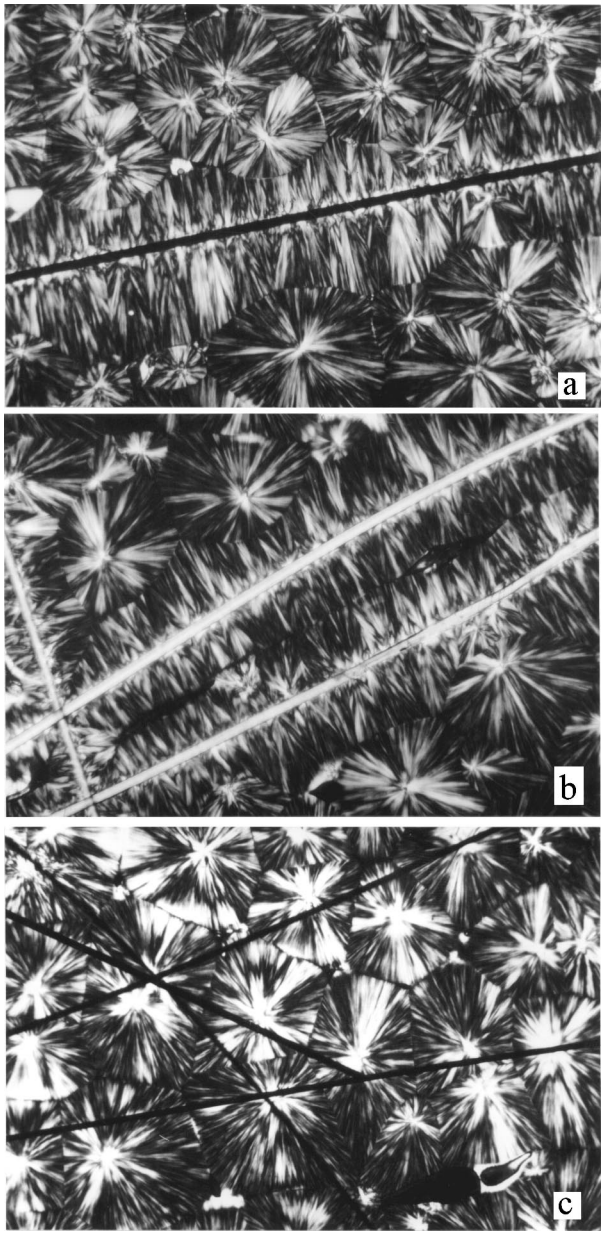

Figure 1 Transmission-polarized optical micrographs of isolated fibers in thin films of 24 MFI PP: (a) pitch-based carbon fiber, diameter 9 μm; (b) Kevlar-29® fibers, diameter 12 μm; (c) PAN-based carbon fibers, diameter 8 μm.

unoriented. Fig. 2 also presents a plot of scattered intensity as a function of scattering angle (2θ). From this plot, the α–PP reflections can be indexed as the (1 1 0) at $2\theta = 14.1^\circ$, the (0 4 0) at $2\theta = 16.9^\circ$, the (1 3 0) at $2\theta = 18.5^\circ$, the (1 1 1) at $2\theta = 21.4^\circ$, and the ($-$1 3 1) at $2\theta = 21.8^\circ$ [15]. These indices are based on a monoclinic α–PP unit cell with parameters $a = 0.665$ nm, $b = 2.096$ nm, and $c = 0.650$ nm with the monoclinic angle (β) between the a and c-axis equal to 99.33° [13]; these dimensions were used in all calculations described below. The small shoulder near $2\theta = 16^\circ$ in Fig. 2 indicates the presence of a small amount of β–phase PP in the unreinforced sample; the strongest β–PP reflection, the (300), occurs at $2\theta = 16.1^\circ$ [15]. However, there was no indication of this or any other β–PP reflections in any of the WAXS patterns from the composites. The dashed line below the (1 1 0) reflection in Fig. 2 indicates the background level that was subtracted before analyzing the crystalline portion of the signal.

The 2-D WAXS pattern obtained from the 24 MFI PP matrix reinforced with 28 vol % pitch-based carbon fibers is shown in Fig. 3. The WAXS image is a superposition of the reflections from the unit cell of the PP matrix and the scattered intensity from the fibers themselves. The fibers show strong (0 0 2) reflections on the equator at $2\theta = 27.4^\circ$, while reflections from the matrix appear at smaller diffraction angles. The azimuthal orientation distribution of the PP reflections indicates a high degree of matrix orientation, even though the specimen was crystallized quiescently. Orientation which resembles transcrystallinity on the micron scale has also been reported after shearing of the PP melt or in the presence of a temperature gradient across the matrix/fiber interface [1]. However, the composite samples investigated in this study were crystallized under quiescent conditions within a closed aluminum mold, thus ruling out the above causes.

As can be seen in the Fig. 3 pattern, the innermost reflection, (1 1 0), is most intense near the meridian with some intensity on the equator. The next PP reflection, (0 4 0), is most intense on the equator with virtually zero intensity on the meridian. These azimuthal intensity variations can be used to construct a model which describes the average orientation of the PP unit cell within the TCL at the fiber-matrix interface.

3.2.2. Model of TCL orientation

An idealized model of this orientation is presented in Fig. 4. Two sets of oriented lamellae are shown; this "cross-hatched" structure occurs in PP because secondary lamellae ("daughters") are able to nucleate and grow from a previously formed lamella ("parent") [13, 14]. The driving force behind this branched growth is the epitaxial match that exists between the a and c unit cell parameters in PP. The model of Fig. 4 would predict all the (0 4 0) intensity on the equator, since for both parents and daughters, the b-axis is perpendicular to the fiber axis. For the (1 1 0) reflection, the same model predicts that the parent lamellae would diffract on the equator (as the c axis is parallel to the fiber axis), while the daughter lamellae would diffract near the meridian (as the c axis is roughly orthogonal in the parent and daughter lamellae). These azimuthal variations for the (1 1 0) and (0 4 0) intensities are indeed consistent with the data in Fig. 3; a more quantitative treatment is described below, but first we consider how the texture depicted in Fig. 4 could arise.

In Fig. 4, the parents are shown growing radially outward from the fibers, which is necessary for their (0 4 0) reflection to appear on the equator. This orientation is postulated to arise from the known epitaxial match between the unit cell of α–PP and the basal plane of graphite [22]; the surface layer in carbon fibers has the graphite basal planes preferentially exposed [21]. Two-dimensional WAXS patterns of carbon fibers have shown that the (1 0 $\bar{1}$ 0) reflection of graphite is most intense on the meridian of flat film images, indicating

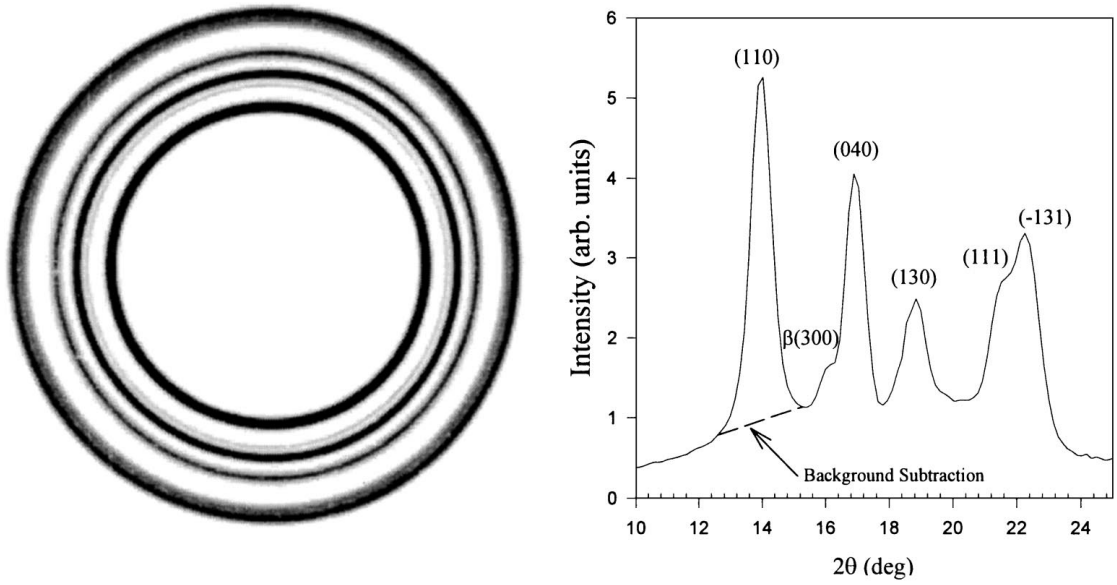

Figure 2 (left) 2-D WAXS pattern of unreinforced 24 MFI PP, molded under same processing conditions as composites. Constant azimuthal intensity for each reflection indicates isotropic nature of specimen. (right:) Intensity as a function of scattering angle (2θ) from 2-D WAXS pattern with α–PP reflections indexed. The dashed line below the (1 1 0) reflection indicates the amorphous background intensity subtracted before analyzing the crystalline portion of the signal.

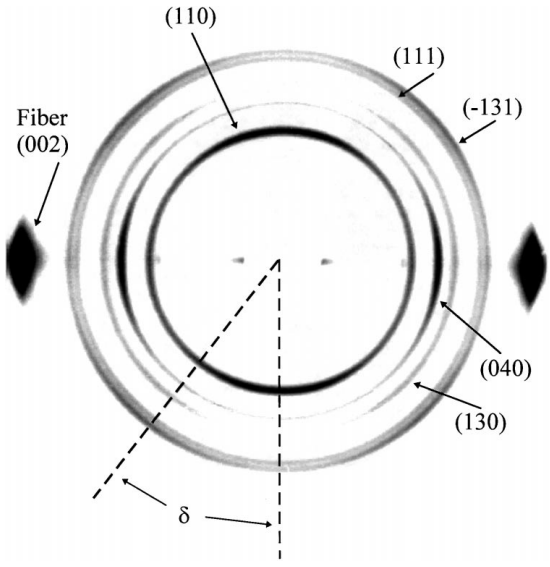

Figure 3 2-D WAXS pattern from 24 MFI PP reinforced with 28 vol % pitch-based carbon fibers. Azimuthal-intensity variations reveal the oriented nature of the PP matrix. Fiber axis is vertical.

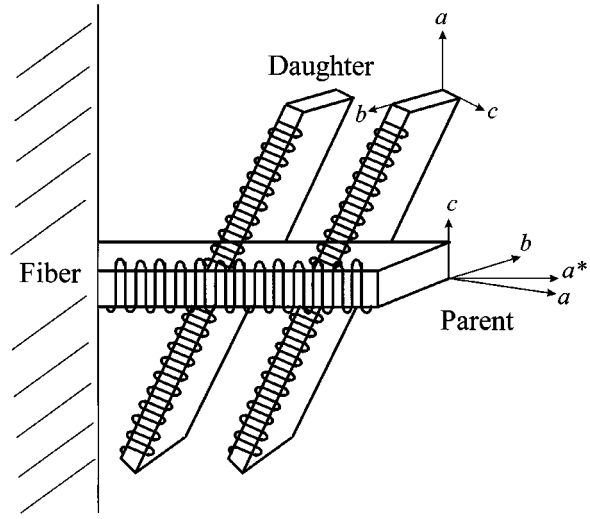

Figure 4 Idealized model for structure within transcrystalline layer (TCL). Model incorporates daughter lamellae growing from an initially-formed parent. *a*, *b*, and *c* represent the unit cell axes of α–PP with a^* representing the component of *a* which is orthogonal to the *b* and *c* axes of the PP monoclinic unit cell.

that the graphite basal planes have longer-range order along the fiber axis than in the transverse direction [23]. Similar WAXS patterns were obtained from the pitch-based carbon fibers used in this study. Thus, our WAXS data can be interpreted by picturing domains of the epitaxially matching surface forming uninterrupted segments along the fiber axis, segments which are longer than a critical nucleus size, whereas transverse to the fiber axis this persistence length is shorter than the critical nucleus size. Consequently, though the unit cell of the graphite basal plane has sixfold symmetry, epitaxial growth occurs only when the PP crystal stems (*c*-axis) lie roughly parallel to the fiber axis. We note that our WAXS results are not consistent with the epitaxial model postulated by Greso and Phillips from studies on different pitch-based carbon fibers, where the match is considered to be with the graphite edge planes [24]. In the Greso and Phillips match, the PP *c*-axis makes an angle of $\pm 78^\circ$ with the carbon-fiber axis, which would lead to a four-spot (0 4 0) reflection 17.1° on either side of the meridian of a flat plate WAXS pattern, well off the equator.

Having established the qualitative texture in our composites, we move on to quantitatively examine the azimuthal intensity variations for the different reflections and their consistency with the model of Fig. 4. Fig. 5 presents the azimuthal trace of the (1 1 0) α–PP reflection from the WAXS pattern in Fig. 3, showing that the cross-hatched structure creates two sets of oriented crystal populations. PP unit cells within the daughter lamellae of the model in Fig. 4 are calculated to produce

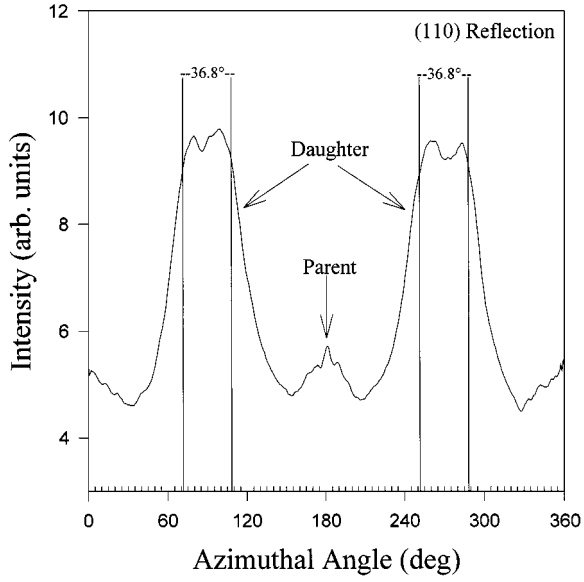

Figure 5 Azimuthal trace of PP (1 1 0) reflection from WAXS pattern of Fig. 3. Azimuthal intensity distribution shows two sets of peaks, one straddling the meridian (90° and 270°) and the other directly on the equator (0°, 180°, and 360°). The calculated locations for the diffracted intensity from the daughter lamellae, following the idealized model of Fig. 4, are marked at 36.8° about the meridian.

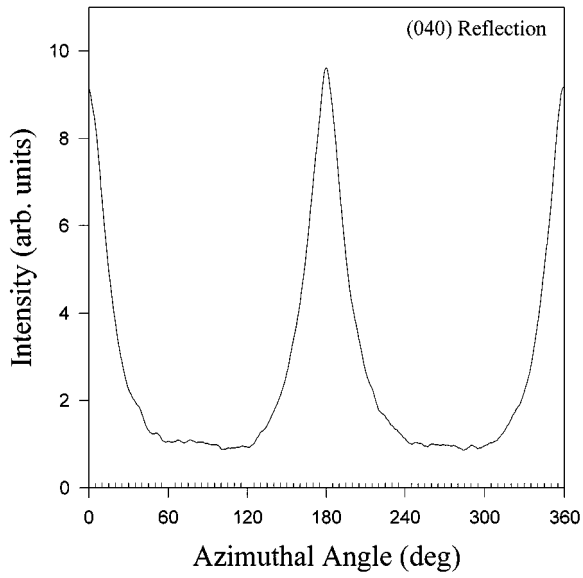

Figure 6 Azimuthal trace of PP (0 4 0) reflection from WAXS pattern of Fig. 3. Both the "daughter" and "parent" lamellae are calculated to show the (0 4 0) reflection on the equator (0°, 180°, and 360°) of the flat plate pattern, as observed.

(1 1 0) reflections 36.8° about the meridian, while the parent lamellae produce reflections on the equator. The calculations concerning the locations of the (1 1 0) and other reflections are presented in Appendix A.2, where the separation angle about the meridian is denoted 2δ; for equatorial reflections $2\delta = 180°$. Fig. 6 shows the azimuthal intensity distribution for the (0 4 0) reflection; the oriented portion of the signal is positioned entirely on the equator (0°, 180°, and 360°), as expected for the model of Fig. 4. The (1 3 0) data, shown in Fig. 7, consist of an oriented signal which spans a much larger range of azimuthal angles. The calculated azimuthal locations of the (1 3 0) reflections, according to the

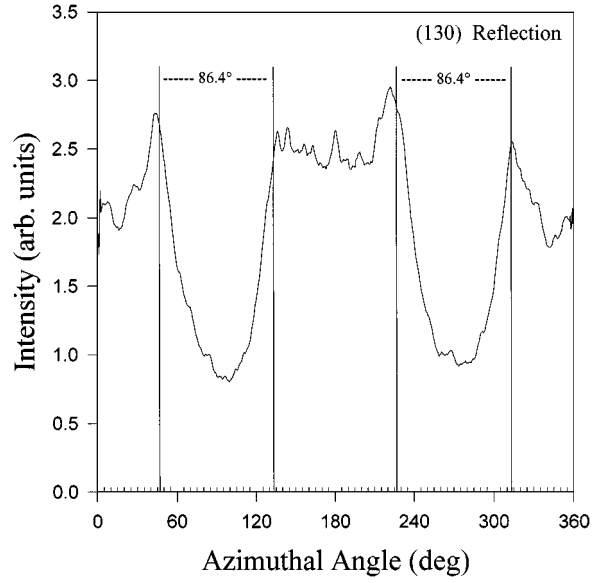

Figure 7 Azimuthal trace of PP (1 3 0) reflection from WAXS pattern of Fig. 3. The calculated location for the diffraction from the daughter lamellae of the idealized TCL model are marked at 86.4° about the meridian.

idealized model of Fig. 4, are marked, where $2\delta = 86.4°$ for the daughter lamellae and $2\delta = 180°$ for the parent lamellae.

Clearly, the model presented in Fig. 4 is a highly idealized case, and while Figs 5–7 show that the model captures the general features of the data, the agreement is not quantitative. In the real case, some deviation of the lamellae (twisting and curving) from their ideal positions would be expected. Moreover, while the model of Fig. 4 is intended to describe the TCL, the actual WAXS data also include any contribution from matrix-nucleated material, which should be roughly isotropic. Assessing the fraction of transcrystallized material in the bulk composite is the main goal of this work, so we address this issue first.

3.2.3. Quantifying the transcrystalline fraction

The level of matrix orientation can be calculated by obtaining the area under the oriented portion of the azimuthal signal relative to the area under the unoriented baseline. This unoriented baseline for the azimuthal data has a single value for each individual reflection and by definition does not vary as a function of azimuthal angle. The (0 4 0) reflection has a much more discernable baseline than do the (1 1 0) and (1 3 0) reflections (Figs 5 and 7), for which the baseline level becomes difficult to locate because of the azimuthal overlap of the contributions from parent and daughter lamellae. Because of this overlap in the (1 1 0) and (1 3 0) data, it is convenient to first use the (0 4 0) data to calculate the level of orientation of the PP matrix. Using this information, either the (1 1 0) or (1 3 0) data can be used to determine the ratio of "daughters" to "parents", with one of the datasets being used to check the model fit of the other.

From the (0 4 0) data shown in Fig. 6, it is a simple matter to calculate the areas under the unoriented

baseline and under the oriented peaks on the equator. In practice, this calculation can be facilitated by fitting Lorentzian curves to the oriented portion of the signal. However, the fraction of transcrystallinity is *not* simply equal to the area ratio, due to differences in the distribution of (0 4 0) plane normals in the oriented and unoriented cases. For the unoriented case, poles for any reflection are distributed randomly over the reciprocal lattice sphere, while for the oriented case, they are distributed in bands at various latitudes. The detailed calculation of these weighting factors is described in Appendices A2 and A3. With the appropriate weightings, the data of Fig. 6 indicate that the fraction of the PP matrix oriented in the general mode shown in Fig. 4 is 0.93, with the remainder being unoriented.

To properly describe the (1 1 0) and (1 3 0) data, and to derive a daughter : parent ratio therefrom, the rigid orientations shown in Fig. 4 need to be relaxed somewhat. The azimuthal intensity profiles are directly related to the angle (ϕ), which a PP unit cell's lattice plane normal makes with the symmetry axis (fiber axis) of the composites. For the idealized model of Fig. 4, the daughter lamellae have $\phi_{(1\,1\,0)} = 19.7^\circ$, $\phi_{(0\,4\,0)} = 90.0^\circ$, and $\phi_{(1\,3\,0)} = 44.0^\circ$, and for all three reflections $\phi = 90^\circ$ for the parent lamellae. The specific relationship between ϕ and the measured azimuthal location of a reflection is given in Appendix A.2. If the lamellae twist about the a^*-axis and curve about the b-axis of the PP unit cell from the positions indicated in Fig. 4, they will create a spread of ϕ values, broadening and possibly shifting the azimuthal locations of the reflection maxima from the calculated values shown in Figs 5 and 7. As can be seen in Fig. 5, the azimuthal (1 1 0) separation angle ($2\delta = 36.8^\circ$) for the daughter lamellae calculated from the idealized model is too large to accurately model the (1 1 0) data. So, refinements are needed that will not only produce an apparent (1 1 0) separation angle that is less than 36.8°, but also correctly locate the azimuthal maxima of the (1 3 0) reflection and maintain the (0 4 0) reflection on the equator of the pattern.

The (0 4 0) reflection in Fig. 6 indeed shows an azimuthal breadth of roughly ±20° about the equator of the WAXS pattern. A schematic depiction of the refined model for the TCL is shown in Fig. 8, indicating how the PP lamellae may curve and twist. A ±20° twist in the PP parent lamellae about their fast growth axis (a^*) would produce a $\phi_{(0\,4\,0)}$ range of 90° ±20° and thus would yield a $\delta_{(0\,4\,0)}$ range of 90° ±20° for both the parent and daughter lamellae. This type of lamellar twist also affects the distribution of the (1 1 0) and (1 3 0) plane normals. To calculate the (1 1 0) plane normal distribution, the value of the unoriented baseline intensity for the (1 1 0) reflection must be found. This can be accomplished by using the result of the (0 4 0) analysis, where 7% of the matrix was found to be unoriented, and applying the appropriate weighting factors as detailed in Appendices A.2 and A.3.

To model the oriented portion of the (1 1 0) reflection, the (1 1 0) plane normals for the daughter contribution are allowed to vary with a Gaussian distribution about the idealized value of $\phi = 19.7^\circ$. This symmetric movement in the (1 1 0) plane normal actually yields an asymmetric shift in the azimuthal intensity maxima due to the weighting functions (as discussed in Appendix A.3), decreasing the splitting angle across the meridian (2δ) from the idealized value of 36.8° shown in Fig. 5. Fig. 9 shows the refined model fit overlayed with the (1 1 0) azimuthal intensity data. For computation of the daughter contribution, the Gaussian distribution about $\phi = 19.7^\circ$ was divided into 15 parts; to smooth out this discretization, each of these parts was then set to be a Lorentzian of equal breadth and height corresponding to its position within the Gaussian distribution. Each of the 15 parts of the distribution was given a separation angle (2δ) determined from the location of the (1 1 0) plane normal within the Gaussian distribution. To describe the diffraction from the parent lamellae, a set of Lorentzian curves, centered on the equator (0°, 180°, and 360°), was added. The fit shown in Fig. 9 was obtained by fixing the level of the unoriented baseline at 0.40, in the intensity units of the figure, and then summing together the daughter and parent contributions, regressed

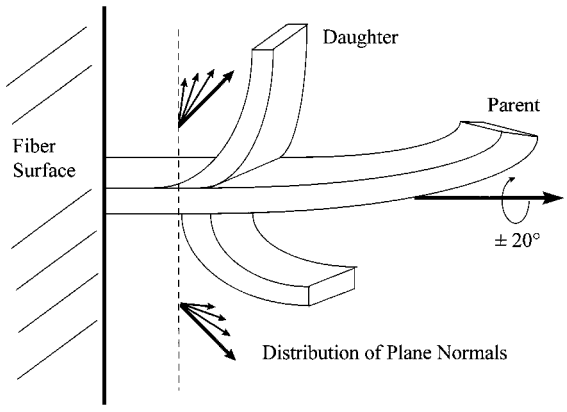

Figure 8 Refined model for the transcrystalline layer (TCL) at the fiber/matrix interface, allowing for some twisting and curving in the growth of parent and daughter lamellae.

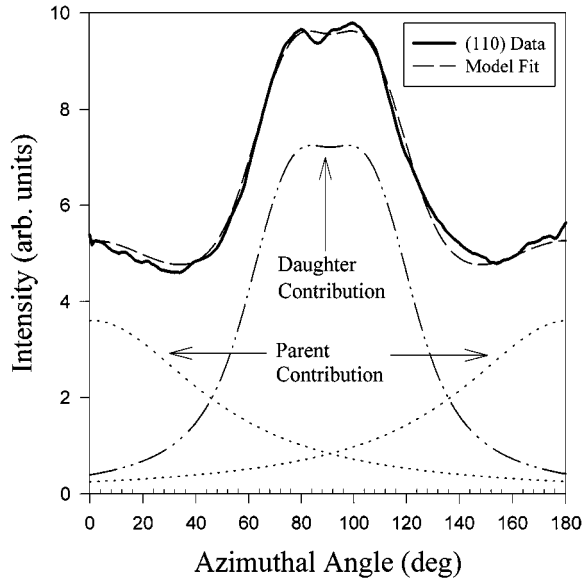

Figure 9 Azimuthal trace of (1 1 0) reflection from WAXS pattern of Fig. 3 with model-fit overlay. Plot shows "parent" and "daughter" contributions, which are added to the baseline level (0.40 intensity units) to produce the final model fit.

using a Marquardt-Levenberg algorithm. The curve-fitting process thus employed four floating parameters (daughter : parent ratio, Gaussian breadth for daughter-pole distribution, Lorentzian breadth for parents, and Lorentzian "smoothing" breadth for each element of the Gaussian-daughter distribution), though fixing the last of these four at an average value (see Appendix A.3) gave essentially identical results. This refined model produces an excellent fit to the data, unlike the idealized model of Fig. 4. From the fit in Fig. 9, using the appropriate weighting factors as described in Appendix A.3, the ratio of daughter to parent material is found to be 0.40. This is within the range (0.33 to 0.5) previously estimated for PP from birefringence measurements [13]. Our technique provides a direct measurement of this daughter : parent ratio, which has been reported to play a role in the long flex life of polypropylene specimens [25]. Simple integration of the "daughter" and "parent" peak areas in Fig. 9 would suggest a daughter to parent ratio much *greater* than unity, indicating the importance of correctly calculating the weighting factors.

To further confirm the model of Fig. 8, the (1 3 0) azimuthal data were examined. Because the daughter and parent contributions lie so close to one another azimuthally, the breadth for each of the Lorentzians representing the (1 3 0) parent contribution to the scattered intensity was rigidly set at the value calculated for the parent contribution of the (1 1 0) fit. The (1 3 0) fit was then calculated in a similar manner to that for the (1 1 0) data, but allowing the unoriented baseline intensity to vary as well, for a total of four floated parammeters (daughter : parent ratio, Gaussian breadth for daughter pole distribution, baseline level, and Lorentzian "smoothing" breadth for daughters). Fig. 10 shows the (1 3 0) azimuthal data with the calculated fit; the unoriented baseline was found to be 0.13 in the intensity units of the figure. Thus, this fit provides an independent estimate of both the fraction of transcrystallized material and the daughter : parent ratio; these are found to be 0.95 and 0.36, respectively, which are in excellent agreement with the values of 0.93 (from the (0 4 0) data) and 0.40 (from the (1 1 0) data). This confirms the validity of the model and its utility in quantifying the level of transcrystallized material in a bulk composite.

3.2.4. Transcrystalline orientation: Kevlar fibers

Although the orientation of the PP matrix is more pronounced in the composites reinforced with the pitch-based carbon fibers, the Kevlar-29 samples showed a qualitatively similar orientation. Fig. 11 presents the 2-D WAXS pattern obtained from the 24 MFI PP reinforced with 31 vol % Kevlar-29 fiber, while Fig. 12

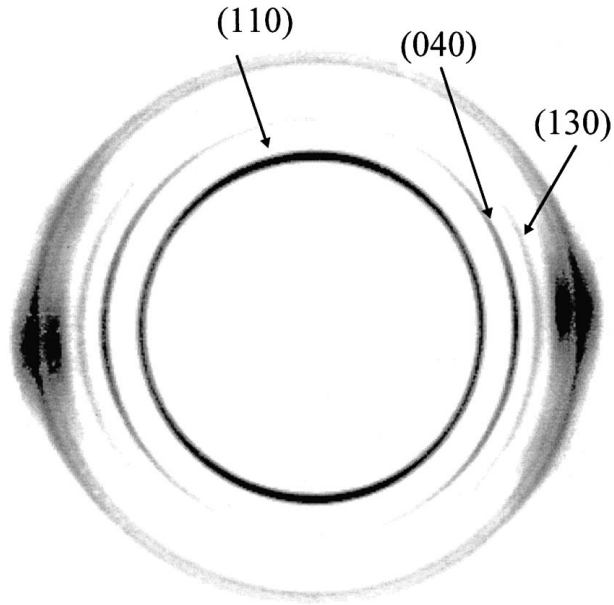

Figure 11 2-D WAXS pattern from sample of 24 MFI PP reinforced with 31 vol % Kevlar-29 fiber. Orientation of PP reflections qualitatively similar to that in pitch-based carbon fiber reinforced composites.

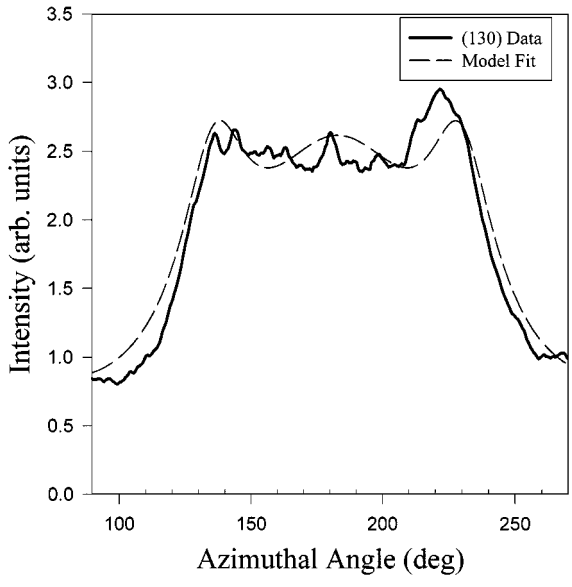

Figure 10 Azimuthal trace of (1 3 0) reflection from WAXS pattern of Fig. 3 with model-fit overlay. Fit based on refined model of Fig. 8, which allows for distribution of plane normals.

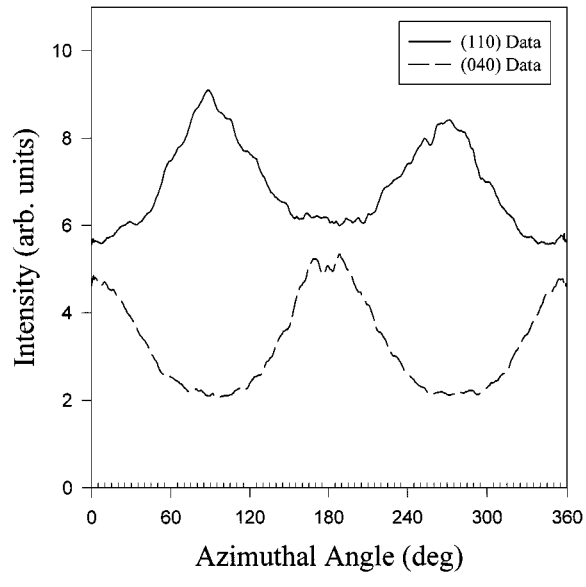

Figure 12 Azimuthal traces of (1 1 0) and (0 4 0) reflections from the 2-D WAXS pattern of Fig. 11. This Kevlar-29 reinforced composite shows an orientation qualitatively similar to that in the pitch-based carbon-fiber composites but with a much broader azimuthal spread.

depicts the (1 1 0) and (0 4 0) azimuthal traces. The orientation of the PP reflections is indeed similar to that seen in the pitch-based carbon data. The relatively weak orientation found in the Kevlar-29 composites complicates the modeling; note that the (1 1 0) azimuthal-intensity distribution in Fig. 12 has the equatorial contribution (0°, 180°, 360°) from the parent lamellae virtually washed out by the overlap of the peaks from the daughter lamellae (near 90° and 270°). However, the (0 4 0) reflection can still be used to obtain the fraction of transcrystallized material in these Kevlar composites simply by representing the oriented contribution by a Lorentzian of adjustable breadth.

Kevlar and pitch-based carbon fibers produce a similar orientation of the PP matrix because there is a similar epitaxial match in both systems, here between the *bc*-plane of α–PP and the *ac*-plane of a Kevlar unit cell. The reported unit-cell dimensions for α–PP are $b_{PP} = 2.096$ nm and $c_{PP} = 0.650$ nm [13], while for Kevlar, $b_K = 0.520$ nm and $c_K = 1.290$ nm [2]. Hence, $2(c_{PP}) = c_K$ and $4(b_K) = b_{PP}$ to within 0.8%. As with the epitaxial match of PP and the pitch-based carbon fibers, the match with the Kevlar unit cell is also consistent with the *c*-axis of PP lying parallel to the fiber axis (*c*-axis) of Kevlar [2]. The poorer orientation of the TCL observed in the Kevlar composite WAXS data relative to the pitch-based carbon fiber composite data, indicates that the nucleating efficiency of the Kevlar surface is evidently not as great as that of the pitch-based carbon fibers. This conclusion is also supported by differential scanning calorimetry (DSC) data [26], which show that the crystallization rate of the PP matrix at 130°C within Kevlar composites is approximately 1.9 times slower than within pitch-based carbon fiber-reinforced composites.

3.3. Constrained growth orientation

Fig. 13 shows the 2-D WAXS pattern from 24 MFI PP reinforced with PAN-based carbon fibers. Although the PAN-based carbon fibers do not readily nucleate either of the PP matrices, the 2-D WAXS patterns from quiescently crystallized unidirectional composite samples that contain these fibers still indicate an orientation of the PP matrix. However, the PP orientation in the PAN-based carbon composites is qualitatively different from that seen in the pitch-based carbon and Kevlar-29 reinforced systems. In Fig. 13, the WAXS pattern shows the maximum (0 4 0) intensity on the meridian of the pattern, which can be contrasted with the orientation present in the pitch-based carbon fiber composite patterns of Figs 3 and 11, where the (0 4 0) has its maximum intensity on the equator. A pattern similar to Fig. 13 was obtained from PP reinforced with e-glass fibers. Unfortunately, e-glass readily absorbs Cu-Kα X-rays, yielding a poor signal/noise ratio.

As can be seen in Fig. 1, unconstrained spherulites of PP homopolymer grow to diameters of 50 to 100 μm under these crystallization conditions, while interfiber distances within the composite are on the order of 10 μm. Consequently, the fibers constrain the growth of polypropylene spherulites nucleated in the bulk; since

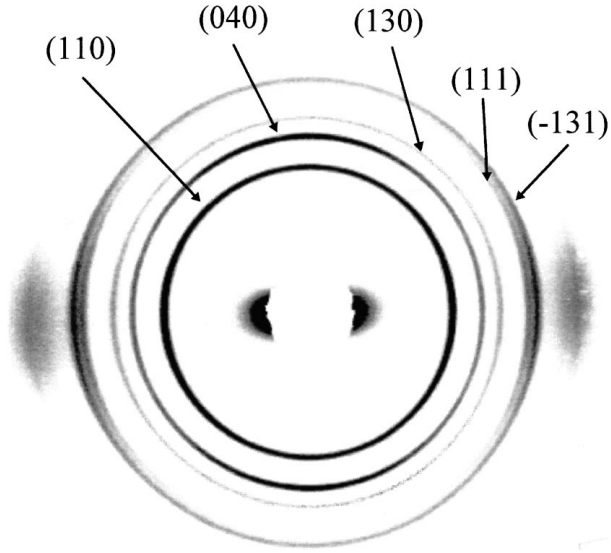

Figure 13 2-D WAXS pattern from 24 MFI PP reinforced with 33 vol % PAN-based carbon fibers. Although this system does not produce a TCL at the fiber/matrix interface, an orientation of the PP matrix is apparent. The (0 4 0) reflection is more intense on the meridian in contrast to the equatorial maximum in the transcrystallizing systems of Figs 3 and 11.

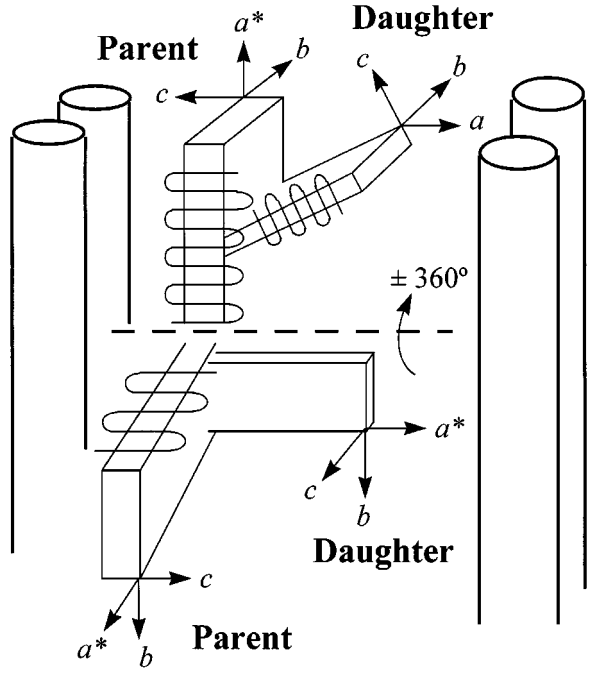

Figure 14 Constrained-growth model depicting parent and daughter lamellae growing from a nucleation site within the matrix. Parents with *c*-axial orientation (not shown) are disfavored.

the fibers are themselves oriented, this can impose an orientation on the crystallites growing between them. Fig. 14 presents a model of this "constrained growth" (CG) orientation. Essentially, parent lamellae having their a^*-axis oriented along the fiber axis can grow relatively freely, growing large in the a^* direction. Those with their *b*-axis oriented along the fiber axis can similarly grow large in the *b* direction. However, those with their *c*-axis oriented along the fiber axis will have their growth in both the a^* and *b* directions restricted by the fibers, while growth in the *c* direction is limited to the lamellar thickness. Consequently, the CG orientation should yield a distribution of plane normals in

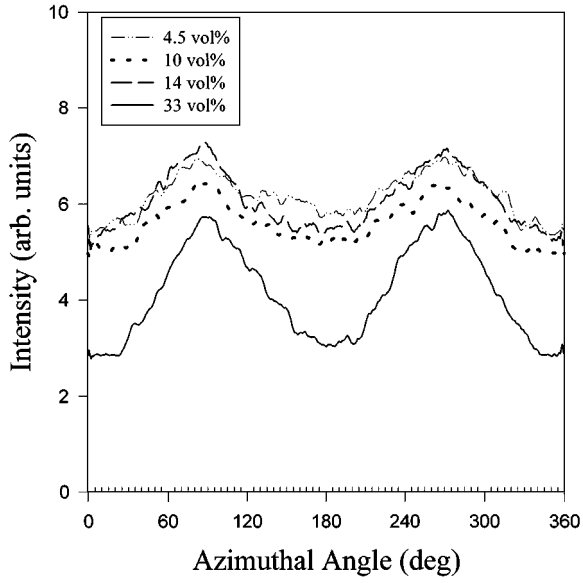

Figure 15 Azimuthal (0 4 0) intensity traces for 24 MFI PP reinforced with PAN-based carbon fibers. Greater intensity on meridian (90° and 270°) results from the "constrained growth" schematically shown in Fig. 14.

which unit cells with *c*-axial orientation are suppressed. In other words, the CG structure can be thought of as consisting of only the axial "cores" of the spherulites, where the equatorial regions are truncated by the presence of the fibers. This produces an (0 4 0) reflection weak on the equator (strong on the meridian), as observed in Fig. 13. The (0 4 0) azimuthal intensity data presented in Fig. 15 for a 24 MFI PP matrix reinforced with PAN-based carbon fiber confirm this, because the more intense regions at azimuthal angles of 90° and 270° correspond to the meridian of the WAXS pattern. Moreover, the azimuthal variation becomes more pronounced as the loading of PAN-based carbon fiber is increased, indicating a progressively greater degree of constraint on the spherulitic growth. The calculations presented in Appendix A4 also indicate that the (1 1 0) and (1 3 0) reflections for the CG orientation would be relatively unoriented, as observed in the data of Fig. 13 (the modest enhancement of intensity on the equator is due to the equatorial "fiber streak" of the PAN-based carbon fibers). Further confirmation of this constrained-growth model comes from tilting the composite sample with respect to the X-ray beam. When the top of the composite specimen is tilted towards the image plate, the intensity of the (0 4 0) on the upper meridian weakens; when the sample is further rotated so that the fiber axis is parallel to the x-ray beam, the resulting WAXS pattern is unoriented as expected.

Since both pitch-based and PAN-based carbon fibers have the graphite basal plane exposed at the surface, it might seem surprising that the PAN-based carbon fibers have no nucleating ability for polypropylene. This difference is doubtless related to the difference in the coherence length of the graphite basal planes at the surface. Hobbs [22] originally studied two PAN-based fibers with different thermal treatments, such that in one specimen the coherence length was only 2.5 nm, while in the other it was > 10 nm. The fiber with the shorter coherence length showed no nucleating capacity, while that with the longer coherence length produced transcrystalline regions similar to what we observe in Fig. 1a; from this, Hobbs concluded that the size of the critical nucleus was in the neighborhood of 5 nm. X-ray diffraction measurements [23] on PAN-based carbon fibers essentially identical to ours indicate a coherence length of 3.1 nm, while for pitch-based carbon fibers with moduli similar to ours, the coherence length is 31 nm. Consequently, the PAN-based carbon fibers can produce only the "constrained growth" orientation, despite their chemical and basic structural similarity to the pitch-based carbon fibers.

3.4. Quantification of orientation

Given that the average interfiber spacing in our composites is on the order of 10 μm, and the thickness of the transcrystalline layers observed for Kevlar-29 and pitch-based carbon composites is roughly 50 μm in Fig. 1, it might be expected that composites containing nucleating fiber would be predominantly composed of transcrystalline material. However, as fiber-loading levels decrease, crystalline matrix material nucleated in the bulk would become progressively more significant. If both fiber-surface and bulk nucleation of the PP matrix take place, both the TCL and CG orientations would coexist. Thus, to quantify the relative amounts of matrix orientation in these composite systems, a method for separating the TCL and CG contributions must be developed. Although the (1 1 0), (0 4 0), and (1 3 0) α–PP reflections are all useful in establishing how the crystallized PP molecules arrange themselves within the composite's matrix, the (0 4 0) reflection is ideally suited for quantifying the relative amounts of transcrystalline, constrained growth, and unoriented material within the samples. In the case of composites containing a portion of "constrained" crystallites, the (0 4 0) reflection has a clear azimuthal separation between the transcrystalline contribution (on the equator for both parent and daughter lamallae) and the constrained growth contribution (on the meridian), allowing the relative contributions of each to be identified. Fig. 16 presents the (0 4 0) azimuthal-intensity distributions for a series of pitch-based carbon composites based on the 24 MFI PP where the azimuthal separation of TCL and CG contributions is apparent. For the 28 vol % composite, the entire oriented portion of the WAXS pattern consists of the TCL contribution at 0°, 180°, and 360° azimuthally, while at lower fiber loadings, populations of matrix-nucleated "constrained" crystallites begin to appear which produce the intensity increase on the meridian of the (0 4 0) reflection (90° and 270°). Thus, the entire (0 4 0) azimuthal intensity distribution can be fit with a combination of unoriented, TCL, and CG contributions, and the relative amounts of each can be quantified. Note, however, that the origin of the crystalline CG material is basically the same as that for the unoriented crystalline component of the matrix: both arise from PP material that was nucleated in the bulk, away from the fiber surface. Thus, the separation between "constrained" and "unoriented" contributions is somewhat artificial; there

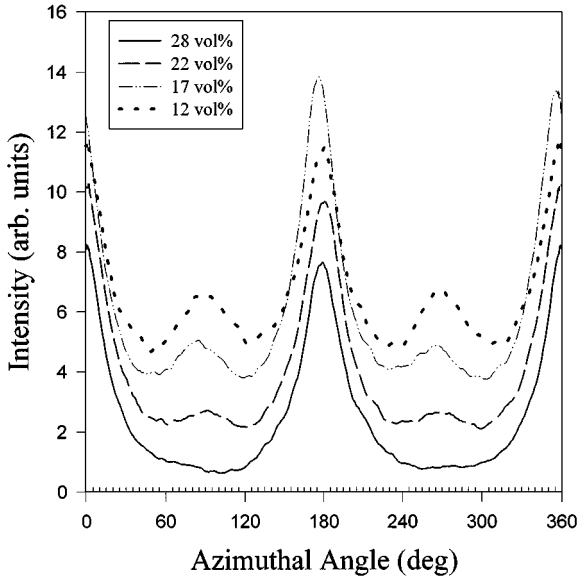

Figure 16 Azimuthal (0 4 0) intensity traces for 24 MFI PP reinforced with pitch-based carbon fibers. Data show appearance of "constrained growth" peak on the meridian (90° and 270°) at low fiber loadings. The TCL contributions for both "parent" and "daughter" lamellae are on the equator.

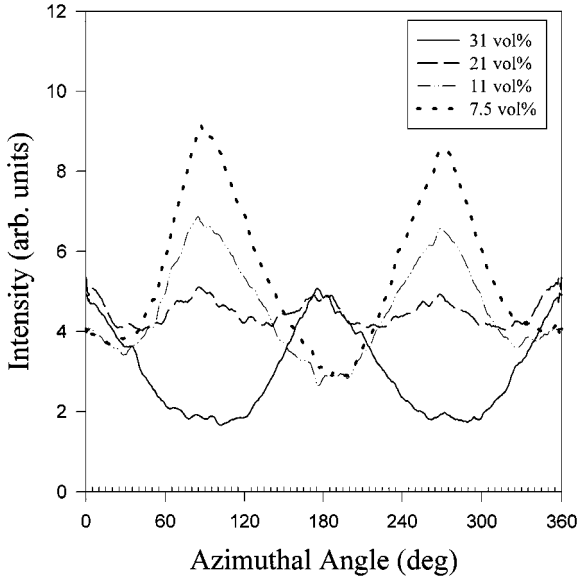

Figure 17 Azimuthal (0 4 0) intensity traces for 24 MFI PP reinforced with Kevlar-29 fibers. Appearance of maxima on the meridian (90° and 270°), from the "constrained growth" orientation, occurs at higher fiber-loading levels than with pitch-based carbon reinforcement. This is consistent with Kevlar fibers being less effective nucleants for the PP matrix, reducing the extent of transcrystallization.

is naturally a distribution of distances from a matrix nucleus to the nearest fiber, and the "constrained" and "unoriented" contributions simply arise from different parts of this distribution.

Fig. 17 presents (0 4 0) data for a series of 24 MFI PP composites reinforced with Kevlar-29, and as previously seen in Fig. 12, the orientation of the PP matrix is not as strong as that seen in the composites reinforced with pitch-based carbon fibers. In fact, at fiber-loading levels below 20 vol %, no clear TCL contribution can be seen in the (0 4 0) data, only that from the CG orientation. Similar data to those shown in Figs 16 and 17 are also obtained with the 400 MFI PP matrix.

By fitting curves to the (0 4 0) azimuthal data and obtaining the appropriately weighted areas corresponding to the TCL, CG, and unoriented contributions, the fraction of transcrystallized matrix can be obtained. This analysis was applied to WAXS patterns from pitch-based carbon and Kevlar-29 reinforced PP composites, at various fiber loadings and for both 24 MFI and 400 MFI matrices. WAXS patterns were acquired from two different locations on each sample. The results of the analysis are presented in Table I. In addition, the daughter : parent ratios were calculated from the two data sets obtained from the highly loaded (30 vol % pitch-based carbon fiber) 24 MFI and 400 MFI matrices. In the case of the 400 MFI composite, the daughter : parent ratio ranged from 0.68 to 0.83, while for the 24 MFI system this value ranged from 0.36 to 0.49. This apparent dependence of the daughter : parent ratio on PP molecular weight is intriguing, but its origin is presently unclear. The transcrystalline fraction (TF) is plotted against fiber loading in Figs 18 and 19. The results for the two matrices (24 and 400 MFI) are quite similar, with the TF being slightly larger for the 400 MFI case. Near 30 vol % loading, pitch-based carbon fibers produce matrix TF values approaching 0.95, while TF values within the Kevlar-reinforced systems are markedly lower. An important result seen in Figs 18 and 19 is that the TF values at low-to-moderate fiber loadings are considerably smaller than would be expected from optical microscopy data of single fibers in a thin PP film. If the fibers in the PP matrix are assumed to be distributed uniformly, and the TCL is assumed to grow at least 40 μm from the fiber/polymer interface as seen in Fig. 1a, all of the pitch-based carbon fiber composites at the 2.5 vol % level and above should have TF values approaching 1.0. However, Figs 18 and 19 show that even at loadings of 20 vol %, the measured TF values are below 0.5, indicating the importance of directly measuring the TCL content in bulk specimens.

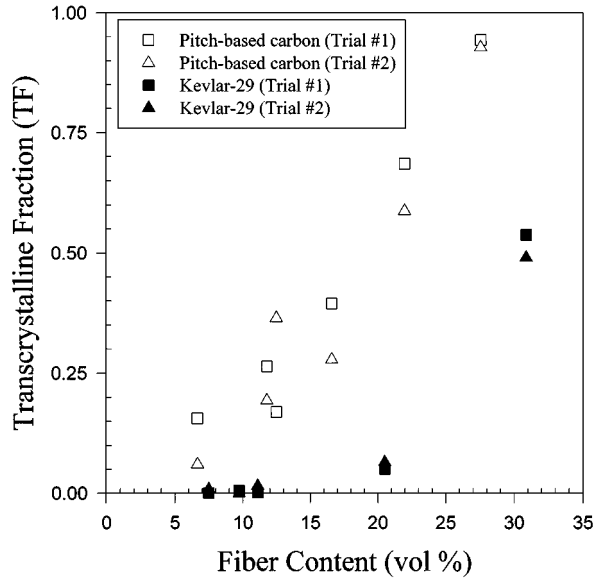

Figure 18 Transcrystalline content of 24 MFI PP-based composites containing varying levels of fiber reinforcement. Measurements based on α–PP (0 4 0) reflection. Squares and triangles indicate replicate measurements from different spots on the composite.

TABLE I Quantification of orientation in pitch-based carbon fiber and Kevlar-29 fiber reinforced composites

Matrix MFI/fiber type	Fiber loading (vol %)	TF trial#1	CGF trial#1	TF trial#2	CGF trial#2	TF (average)
	28	0.93	0.00	0.94	0.00	0.94
	22	0.68	0.00	0.59	0.00	0.64
24 MFI/	17	0.39	0.0057	0.28	0.018	0.34
pitch-based carbon	13	0.16	0.042	0.36	0.0047	0.26
	12	0.26	0.016	0.19	0.032	0.23
	6.7	0.16	0.042	0.061	0.048	0.11
	30	0.89	0.00	1.0	0.00	0.94
400 MFI/	17	0.68	0.00	0.68	0.00	0.68
pitch-based carbon	13	0.18	0.019	0.38	0.0027	0.28
	9.0	0.37	0.0023	0.40	0.00	0.39
	31	0.54	0.00	0.49	0.00	0.51
24 MFI/	21	0.063	0.027	0.064	0.021	0.064
Kevlar-29	11	0.0012	0.17	0.015	0.12	0.0081
	10	0.0055	0.078	0.00	0.13	0.0028
	7.5	0.00	0.44	0.0076	0.19	0.0038
400 MFI/	14	0.065	0.033	0.082	0.014	0.073
Kevlar-29	10	0.016	0.084	0.028	0.064	0.022
	5.1	0.0012	0.10	0.00	0.16	0.0006

*TF = Transcrystalline fraction as measured from (0 4 0) reflections. CGF = Fraction of constrained growth material. TF + CGF + Unoriented = 1.

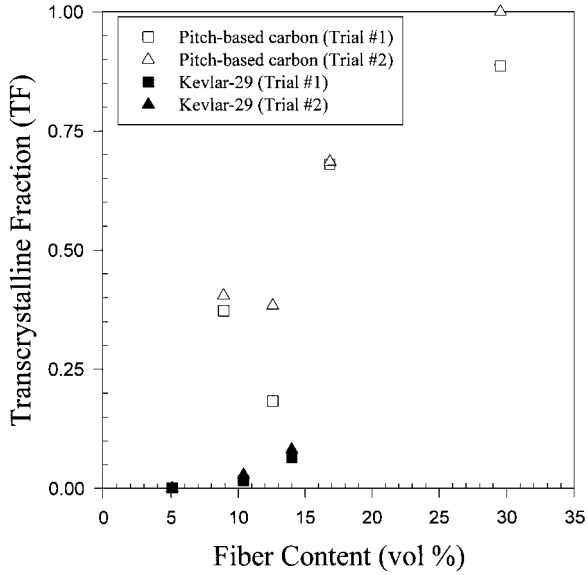

Figure 19 Transcrystalline content of 400 MFI PP-based composites containing varying levels of fiber reinforcement. Measurements based on α–PP (0 4 0) reflection. Squares and triangles indicate replicate measurements from different spots on the composite.

4. Conclusions

Flat plate WAXS patterns effectively reveal the matrix orientation that occurs in unidirectional continuous fiber-reinforced PP composites. From these WAXS images, a model for the transcrystalline layer (TCL) which is nucleated by the surfaces of both pitch-based carbon and Kevlar®-29 fibers was developed. The model incorporates an epitaxial match between the PP unit cell and the graphite and Kevlar unit cells, as well as the epitaxial growth of "daughter" PP lamellae on "parent" lamellae. Furthermore, a previously unreported mode of PP matrix orientation was observed in composites reinforced with PAN-based carbon fibers, which do not nucleate PP, due to restrictions on the growth of PP crystals by the fibers. The extent of this "constrained growth" (CG) orientation increases with fiber loading, as growth restrictions become progressively more severe. Even for pitch-based carbon and Kevlar fibers, this CG orientation was found to coexist with the TCL orientation at lower fiber loadings.

The model was used to quantify the fraction of transcrystallized material in the PP matrix as a function of fiber loading for pitch-based carbon and Kevlar-29 fibers. While the transcrystalline fraction (TF) increases with fiber loading in both cases, at a given volume fraction of fibers, the TF is far higher when pitch-based carbon fibers are used, indicating a much higher nucleating efficiency versus Kevlar. At 30 vol % pitch-based carbon fibers, the TF of the matrix exceeds 0.90, while Kevlar fiber loadings of 15 vol % and below yielded transcrystalline fractions too small to determine reliably. Analysis of the composites with the highest TF values indicated the daughter : parent ratio is 0.36–0.49 for the 24 MFI matrix and 0.68–0.83 for the 400 MFI system, providing a direct measurement of this important quantity.

The quantification method developed in this work should prove useful in directly linking TCL content in fiber-reinforced PP composites to their bulk mechanical properties. Currently, the flexural properties of these composites are being measured and will be reported on in the future.

Appendix: Model calculations

A.1. Location of azimuthal reflection for oriented PP unit cell

We first define a set of orthogonal axes (a^*, b, and c) which represent the α–PP unit cell and are allowed to rotate around a symmetry axis. The symmetry axis will be chosen to coincide with the fiber axis in the composite. The a^*-axis is defined as the component of the a-axis which is perpendicular to the c-axis of the monoclinic α–PP unit cell. The axes of the α–PP unit cell are allowed to rotate by an angle ω about a set of fixed orthogonal axes (x, y, z) which represent the laboratory reference frame. The α–PP unit cell is assumed to be oriented with tilted symmetry with respect to one of the lab-reference axes, as in Fig. 4; that is, there is rotational

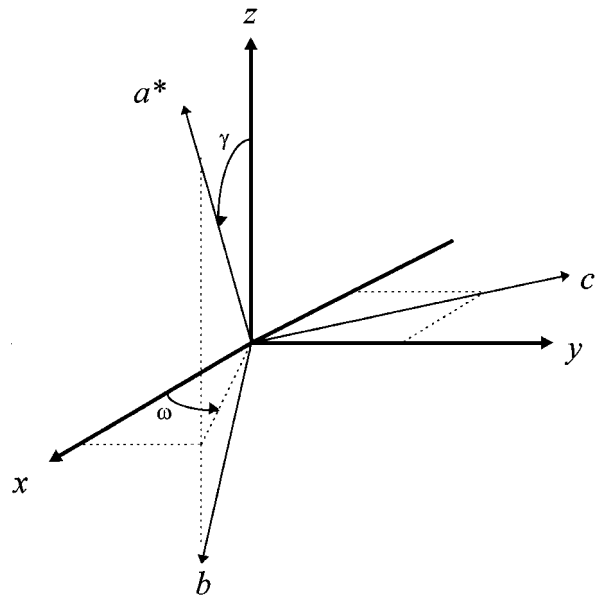

Figure A1 (a^*, b, c) orthogonal system represents the unit cell of α–PP placed in the fixed lab coordinate system of (x, y, z). With the x-ray beam along the y-axis and using a given tilt angle (γ), the unit cell system is allowed to rotate (ω) about the symmetry axis (z) until the Bragg condition is satisfied.

symmetry about the fiber axis, but the lamellae (particularly the daughter lamellae) may be neither parallel nor perpendicular to the fiber axis. This system of axes is pictured in Fig. A1 showing the tilt angle (γ) between the a^*-axis of PP and the z-axis of the fixed reference frame. The X-ray beam is chosen to coincide with the y-axis. While all values of ω are allowed, only particular values produce a position of the unit cell (a^*, b, c) at which the Bragg condition is satisfied. From the values of ω which meet the Bragg condition, the azimuthal location of the reflection on a flat plate pattern can be found.

For example, by setting $\gamma = 0$, we can calculate the azimuthal location of the (1 1 0) α–PP reflection for a unit cell oriented with the a^*-axis parallel to the z-reference axis. The z-axis represents the fiber axis in the composites. First, we write an equation for the (1 1 0) plane normal, $P\vec{n}_{(1\,1\,0)}$, as a function of γ and ω in terms of the fixed laboratory reference frame.

$$\begin{aligned} P\vec{n}_{(1\,1\,0)} = &\left[\left(\frac{1}{\cos(\beta)(a_i)}\right)\cos(90-\gamma)\cos(\omega)\right.\\ &\left.+\left(\frac{1}{b_i}\right)\cos(\gamma)\cos(\omega)\right]\hat{x}\\ &+\left[\left(\frac{1}{\cos(\beta)(a_i)}\right)\cos(90-\gamma)\cos(90-\omega)\right.\\ &\left.+\left(\frac{1}{b_i}\right)\cos(\gamma)\cos(90-\omega)\right]\hat{y}\\ &+\left[\left(\frac{1}{\cos(\beta)(a_i)}\right)\cos(\gamma)\right.\\ &\left.+\left(\frac{1}{b_i}\right)\cos(90+\gamma)\right]\hat{z} \equiv A\hat{x}+B\hat{y}+C\hat{z} \end{aligned} \tag{A1}$$

Here, a_i, b_i, and c_i represent the dimensions of the PP unit cell, and $\hat{x}$, $\hat{y}$, and $\hat{z}$ are unit vectors in the respective directions in the laboratory frame; the X-ray beam points along $\hat{y}$. The monoclinic angle (β) is equal to 99.33° for the unit cell of α–PP [13]. After setting $\gamma = 0$, we can solve the Bragg equation for the appropriate value of ω:

$$\frac{(P\vec{n} \bullet \hat{y})}{\|P\vec{n}\|} = \cos(90-\theta) \tag{A2}$$

For the (1 1 0) PP reflection, the diffraction angle $\theta = 7.063°$, so ω is calculated to be 24.30°. This value can then be used to calculate the azimuthal angle δ between the Bragg reflection and the meridian of the flat plate pattern. Because the z-axis is parallel to the meridian and the x-axis is parallel to the equator of the flat plate pattern, δ can be calculated as:

$$\tan(\delta) = \frac{(\textit{magnitude of } \hat{x} \textit{ component of } P\vec{n})}{(\textit{magnitude of } \hat{z} \textit{ component of } P\vec{n})} = \frac{A}{C} \tag{A3}$$

The result is $2\delta = 31.8°$, which is consistent with previously reported results for this type of orientation [11]. Similar calculations can be made for the various other PP reflections.

A.2. Orientation of idealized and refined TCL models

Although the above procedure will be useful for calculating the azimuthal locations of reflections for the "constrained growth" orientation, a more straightforward method lies in finding the intersection of the diffraction sphere with that of the orientation sphere. This method is described by Kakudo and Kasai [27], where the intersection of these spheres for a system with "tilted" symmetry is found from the following relationship.

$$\cos(\delta) = \cos(\phi)/\cos(\theta) \tag{A4}$$

The parameter ϕ is the angle which the plane normal makes with the symmetry axis of the system. For the orientation example used in the previous section, where the a^*-axis was parallel to the fiber axis, the angle $\phi_{(1\,1\,0)}$ between the (1 1 0) plane normal and the z symmetry axis is calculated to be 17.38°. As expected, using $\phi = 17.38°$ and $\theta = 7.063°$ in Equation A4 gives $2\delta = 31.8°$. For the perfectly oriented daughter lamellae of the model in Fig. 4, the angle that the (1 1 0) plane normal makes with the fiber axis is calculated to be $\phi_{(1\,1\,0)} = 19.7°$, while for the (1 3 0) plane $\phi_{(1\,3\,0)} = 44.0°$. Using these values in Equation A4, the separation angles $2\delta_{(1\,1\,0)}$ and $2\delta_{(1\,3\,0)}$ are calculated to be 36.8° and 86.4° respectively.

Although Equation A4 yields the azimuthal location of a reflection for a given lattice-plane position (ϕ), it is also necessary to understand how the scattered intensity varies with ϕ. To understand this relationship, it is helpful to view the intersection of the orientation (reciprocal lattice) sphere, which depicts the location

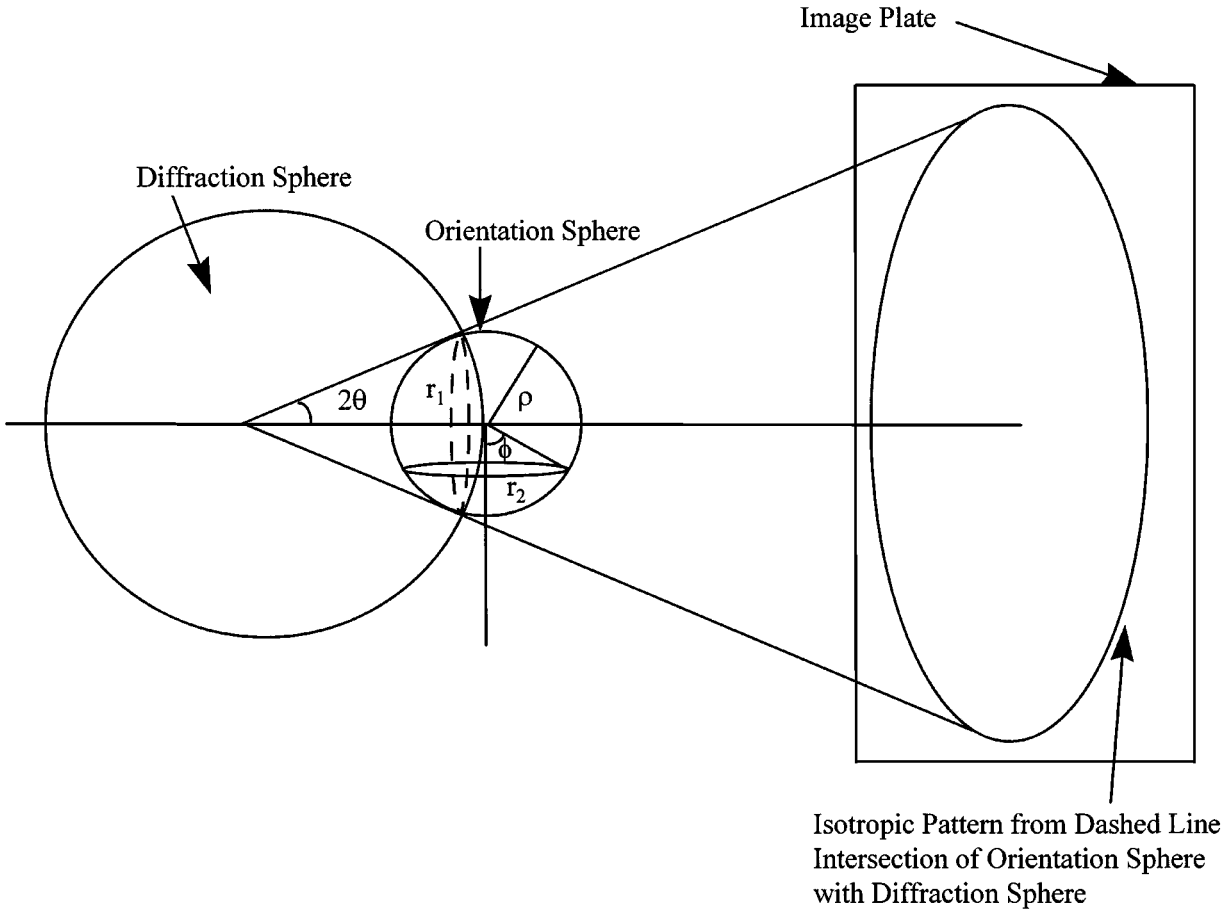

Figure A2 X-ray scattering geometry showing intersection of orientation sphere with diffraction sphere (dashed ellipse, radius r_1).

of the lattice plane normals, with the diffraction sphere as pictured in Fig. A2. This intersection, depicted as a dashed ellipse in Fig. A2, describes where the Bragg condition is satisfied for a given reflection, and hence, where a reflection on the flat plate pattern will appear for a particular value of ϕ on the orientation sphere. From Fig. A2, it can be seen that in a system containing an axis of symmetry from the north to south pole of the orientation sphere (corresponding to the fiber axis in the composites), a given value of ϕ will trace out an orientation cone. If all plane normals have the same value of ϕ, then as ϕ moves to smaller values, the circumference that this cone traces on the surface of the orientation sphere becomes smaller, bunching the normals more tightly together. Since the total number of plane normals is fixed, the density of plane normals on the orientation sphere is much larger when the preferred value of ϕ is near 0°. Because the scattered intensity is proportional to the density of poles at the location on the orientation sphere where the Bragg condition is satisfied, an oriented reflection which occurs on the equator of the flat plate pattern ($\phi = 90^\circ$) will appear less intense than an equivalently oriented distribution of poles nearer the meridian. So, before a refined model incorporating a distribution of plane normal angles (ϕ) can be developed from the azimuthal data, a correction factor describing how the relative intensities for a given reflection vary with ϕ must first be developed.

The relative intensity of an oriented reflection is most conveniently referenced to the intensity that would be measured from an unoriented system, which necessarily has a uniform density of poles covering the entire orientation sphere.

$$\text{Unoriented Pole Density (UPD)} = 2\pi r_1 w / 4\pi\rho^2 \tag{A5}$$

For an oriented system with the axis of symmetry running from the north to the south pole on the orientation sphere:

$$\text{Oriented Pole Density (OPD)} = 2w/2\pi r_2 \tag{A6}$$

The "density" referred to in Equations A5 and A6 is actually the fraction of poles which meet the Bragg condition. In the above equations, r_1 represents the radius of the circle formed by the intersection of the diffraction sphere with the orientation sphere. The quantity w is the finite width of this intersection circle, due to the variation in unit-cell dimension and polychromaticity of the radiation. This quantity is assumed the same for the oriented and unoriented cases, and so will drop out of the calculations below. The radius of the orientation sphere (ρ) is found from Bragg's Law as $\rho = 2\sin(\theta)/\lambda$, where λ is the wavelength of the radiation. In Fig. A2, ρ is depicted along with the radius $r_2 = \rho\sin(\phi)$, which corresponds to the radius of the circle that defines a specific latitude on the orientation sphere. The ratio of r_1 to ρ for the intersection circle depicted in Fig. A2 is given as:

$$f = r_1/\rho = \sin(90 - \theta) \tag{A7}$$

So, for the (1 1 0), (0 4 0), and (1 3 0) reflections, this value of f equals 0.992, 0.989, and 0.987 respectively.

From the above equations, it can be shown that the ratio of oriented to unoriented intensity, when all poles are oriented at an angle ϕ with cylindrical symmetry, is given as:

$$(\text{OPD/UPD}) = 2/[\pi f \sin(\phi)] \equiv P \qquad \text{(A8)}$$

Equation A8 can be used to generate the weighting factors P needed to correct for the increased intensity recorded from plane normals which are oriented nearer the north and south poles of the orientation sphere. In modelling the azimuthal intensity traces, these weighting factors multiply the intensity contributions from the various crystal populations (parent vs. daughter, distribution of pole normal angles, etc.).

A.3. Refined TCL model curve fit

For the three PP reflections that were examined—(1 1 0), (0 4 0), and (1 3 0)—the parent contribution was simply modeled with Lorentzian curves centered on the equator of the flat plate pattern at 0°, 180°, and 360° azimuthally. For these parent lamellae contributions, both the height and the width of the Lorentzians were allowed to vary during the fitting process. For the daughter lamellae contributions to the (1 1 0) and (1 3 0) signal, multiple sets of Lorentzian curves of equal but adjustable breadth were used to fit the data, with each set of curves representing a specific value of ϕ within the plane normal distribution. Fits to the data were also performed by fixing the breadth of the individual Lorentzian daughter curves, which yielded the same TF values to within 4%. Fifteen sets of these Lorentzian curves were used for the (1 1 0) and (1 3 0) daughter lamellae fit, and each was weighted according to the density of poles on the orientation sphere at each location of ϕ, using Equation A8. Thus, the lamellae of the idealized model of Fig. 4 should produce (1 1 0) daughter reflections that are roughly $\sin(90^\circ)/\sin(19.7^\circ)$ or 2.97 times as intense as the (1 1 0) parent reflections.

To describe the breadth of the daughter contributions to the azimuthal (1 1 0) and (1 3 0) traces, the model also allowed for the lamellae to curve and twist as shown schematically in Fig. 8. This meandering was modelled with a Gaussian distribution in plane normal location. Thus, an additional intensity weighting factor for a given value of ϕ was determined from its position within this Gaussian distribution of ϕ relative to the value ϕ_{ideal} calculated from the idealized model of Fig. 4 (19.7° and 44.0° for the (1 1 0) and (1 3 0) reflections). This distribution-weighting factor was represented by the following equation.

$$\text{Distribution Weighting Factor (D)} = \exp\left(-[(\phi - \phi_{\text{ideal}})/2G]^2\right) \qquad \text{(A9)}$$

The parameter G in Equation A9 describes the breadth of the Gaussian distribution in ϕ and was varied during the curve-fitting process. The best-fit value of G was approximately 9° for the (1 1 0) fits and 1° for the (1 3 0) fits.

The relative intensites of the individual sets of Lorentzian curves for each reflection were then weighted in the curve-fitting algorithm, using an overall weighting factor, which was calculated as a function of ϕ from the product of Equation A8 and Equation A9:

$$\text{Overall Weighting Factor (W)} = DP \qquad \text{(A10)}$$

The values of W were multiplied in the curve-fitting algorithm with the height values of the Lorentzian curves.

The actual fitting proceeded as follows: first, Lorentzian curves were fit to the (0 4 0) data to obtain the relative area under the oriented portion of the signal relative to the area under the unoriented baseline. This measure of orientation level was then used during the (1 1 0) fit by fixing the level of the (1 1 0) baseline in order to produce a fit that yielded the same ratio of oriented to unoriented area. From the (1 1 0) fit, which allowed the plane normal location (ϕ) to vary over a Gaussian distribution centered at 19.7°, the breadth of the Lorentzian describing the contribution from the parent lamellae was obtained, and fixed at this value in the (1 3 0) fit. The (1 3 0) fit, which had plane normals that varied over a Gaussian distribution centered at 44.0°, used the (1 1 0) value of parent Lorentzian breadth for its parent-curve contribution while allowing the unoriented baseline intensity to vary. When weighting the areas under the constrained growth contributions to the (0 4 0) signal, Equation A8 was used to calculate a weighting factor (P) at each value of ϕ. Further consideration of the constrained growth model is given in the next section. The above procedure produced the results listed in Table AI for the (0 4 0), (1 1 0) and (1 3 0) reflections in the highly loaded pitch-based carbon fiber-reinforced composites.

A.4. Constrained growth orientation

The "constrained growth" orientation is difficult to model quantitatively because there is a spread of inter-fiber distributions in any composite and because nucleation occurs randomly in the matrix (rather than at the fiber surface, as in the TCL case). Nonetheless, we can roughly approximate the CG orientation by assuming that the *c*-axis of the parent lamellae is perpendicular to the fiber axis (see Fig. 14) and further assuming free rotation of the a^*b plane about *c*. We can then calculate the azimuthal separation angle (δ) between the meridian of the flat plate pattern and the reflection as a function of tilt angle (γ, see Fig. A1) using equations A1, A2 and A3. For the parent lamellae of the CG model, 2δ for the (1 1 0) and (0 4 0) reflections can take on all values from 0° to 180°, and all are roughly equally represented as γ is varied; the results for the (1 1 0) reflection are shown in Fig. A3. Recall that the weighting factors of Equation A8 indicate that the diffracted intensity will be greater as ϕ approaches zero; thus, from Equation A4, the diffracted intensity will be greater as 2δ approaches zero, corresponding to the meridian of the flat plate pattern. Hence, for the unit cells within the CG parent lamellae, as 2δ approaches zero, the diffracted intensity will increase, and both the (0 4 0) and (1 1 0) reflections

TABLE AI Full Model Fit Results for Composites Highly Loaded with Pitch-Based Carbon Fiber

Data Set	Reflection Fit	Baseline Intensity[1]	Parent Lorentzian Breadth[2]	Daughter Lorentzian Breadth[2]	Daughter: Parent Ratio	TCL Fraction
28 vol %	(0 4 0)	0.29	NA	NA	NA	0.93
pitch-based	(1 1 0)	0.40 (fixed)	46.8	16.0	0.40	0.93
carbon	(1 3 0)	0.13	46.8 (fixed)	15.1	0.36	0.95
in 24 MFI PP (Trial#1)						
28 vol %	(0 4 0)	0.21	NA	NA	NA	0.94
pitch-based	(1 1 0)	0.28 (fixed)	41.9	18.1	0.49	0.94
carbon	(1 3 0)	0.016	41.9 (fixed)	16.3	0.45	0.99
in 24 MFI PP (Trial #2)						
30 vol %	(0 4 0)	0.31	NA	NA	NA	0.89
pitch-based	(1 1 0)	0.65 (fixed)	27.10	13.1	0.68	0.89
carbon	(1 3 0)	0.36	27.10 (fixed)	16.4	0.83	0.87
in 400 MFI PP (Trial #1)						
30 vol %	(0 4 0)	0.00	NA	NA	NA	1.00
pitch-based	(1 1 0)	0.02 (fixed)	27.54	12.7	0.71	1.00
carbon	(1 3 0)	0.00	27.54 (fixed)	11.9	0.72	1.00
in 400 MFI PP (Trial #2)						

Notes: 1) Baseline intensity values given in arbitrary units of Figs 9, 10, and 16.
2) Breadth values describe the standard deviation from the mean of the fitted curves.

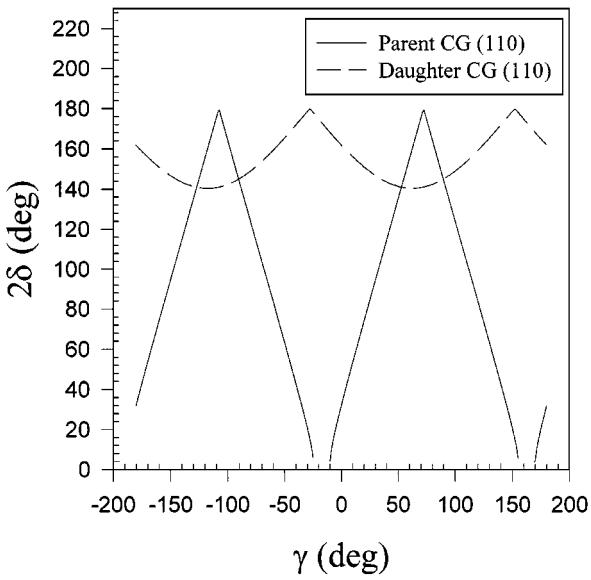

Figure A3 Model calculations for parent and daughter lamellae of constrained-geometry orientation showing separation angle (2δ) about meridian of flat plate WAXS pattern for the (1 1 0) PP reflections as a function of tilt angle (γ).

will appear more intense on the meridian of the pattern. To obtain the properly weighted areas for the CG contribution to the (0 4 0) signal, Equations A4 and A8 were used to calculate a weighting factor at each azimuthal angle.

For the (0 4 0) reflection, the daughter lamellae of the CG orientation show the same 2δ vs. γ behavior as the parent lamellae, thus yielding increased intensity on the meridian. Hence, the parent and daughter lamellae combine to produce an (0 4 0) reflection with maxima on the meridian, as observed in Figs 13 and 15. However, the (h k 0) reflections (h, k $\neq$ 0) for the daughter lamellae of the CG model are a bit more complicated. Fig. A3 shows that the daughter lamellae are calculated to produce (1 1 0) reflections confined to flat plate separation angles 2δ ranging from 140° to 180°. This small range of 2δ confines the daughter (1 1 0) contribution to an area around the equator of the flat plate pattern. Since the observed WAXS pattern contains contributions from both the parent lamellae (more intense near the meridian) and daughter lamellae (which diffract only near the equator), the (1 1 0) and other (hk0) reflections for the CG material are roughly isotropic. Our starting assumption (parent *c*-axis rigorously perpendicular to the fiber axis) is also rather restrictive; relaxing this constraint would further smear out any azimuthal orientation of the (hk0) reflections. Consequently, only the (0 4 0) reflection is useful in quantifying the extent of CG orientation in a unidirectional composite.

Acknowledgements

The authors would like to thank Dr. Roger Phillips of Montell Polyolefins for providing the well-characterized polypropylenes used in this study, and Ms. Sigrid Ruetsch of TRI/Princeton for providing the optical micrographs. The image-plate reader was acquired through support from the National Science Foundation, Polymers Program (DMR-92-57565).

References

1. M. J. FOLKES in "Polypropylene Structure, Blends, and Composites," edited by J. Karger-Kocsis (Chapman & Hall, London, 1995 Vol. 3) p. 340.
2. E. J. H. CHEN and B. S. HSIAO, *Polym. Eng. Sci.* **32** (1992) 280.
3. M. J. FOLKES and S. T. HARDWICK, *J. Mat. Sci.* **25** (1990) 2598.
4. E. G. LOVERING, *J. Polym. Sci. Part A2.* **8** (1970) 1697.

5. T. HATA, K. OHSAKA, T. YAMADA, K. NAKAMAE, N. SHIBATA and T. MATSUMOTO, *J. Adhesion* **45** (1994) 125.
6. V. E. REINSCH and L. REBENFELD, *J. Appl. Polym. Sci.* **52** (1994) 649.
7. L. C. LOPEZ and G. L. WILKES, *Polymer* **29** (1988) 106.
8. G. P. DESIO and L. REBENFELD, *J. Appl. Polym. Sci.* **44** (1992) 1991.
9. N. A. MEHL and L. REBENFELD, *J. Appl. Polym. Sci.* **57** (1995) 187.
10. J. VARGA, *J. Mat. Sci.* **27** (1992) 2557.
11. A. J. LOVINGER, *J. Polym. Sci.: Polym. Phys.* **21** (1983) 97.
12. M. HIKOSAKA and T. SETO, *Polym. Journal* **5** (1973) 111.
13. F. L. BINSBERGEN and B. G. M. DELANGE, *Polymer* **9** (1968) 23.
14. B. LOTZ and J. C. WITTMANN, *J. Polym. Sci.: Part B: Polym. Phys.* **24** (1986) 1541.
15. R. J. SAMUELS and R. Y. YEE, *J. Polym. Sci.: Part A2* **10** (1972) 385.
16. D. R. NORTON and A. KELLER, *Polymer* **26** (1985) 204.
17. S. BRÜCKNER and S. V. MEILLE, *Nature* **340** (1989) 455.
18. S. V. MEILLE, S. BRÜCKNER and W. PORZIO, *Macromolecules* **23** (1990) 4114.
19. R. L. MILLER, *Polymer* **1** (1960) 135.
20. M. GEZORICH and P. H. GEIL, *Polym. Eng. Sci.* **8** (1968) 202.
21. R. N. LEE, in "International Encyclopedia of Composites, Vol. 1," edited by S. M. Lee (VCH Publishers Inc., 1990) 241.
22. S. Y. HOBBS, *Nature* **234** (1971) 12.
23. D. P. ANDERSON and S. KUMAR, *SPE Annual Tech. Conf.* (1990) 1248.
24. A. J. GRESO and P. J. PHILLIPS, *Polymer* **37** (1996) 3165.
25. E. S. CLARK and J. E. SPRUIELL, *Polym. Eng. Sci.* **16** (1976) 176.
26. D. M. DEAN, PhD Thesis, Princeton University (1998).
27. M. KAKUDO and N. KASAI, in "X-ray Diffraction by Polymers" (Elsevier Publishing Co., 1972) 231.

Received 7 December 1997
and accepted 14 July 1998